

An experiment to measure Mie and Rayleigh total scattering cross sections

A. J. Cox, Alan J. DeWeerd, and Jennifer Linden

Citation: [American Journal of Physics](#) **70**, 620 (2002); doi: 10.1119/1.1466815

View online: <http://dx.doi.org/10.1119/1.1466815>

View Table of Contents: <http://aapt.scitation.org/toc/ajp/70/6>

Published by the [American Association of Physics Teachers](#)

Articles you may be interested in

[Particle size determination: An undergraduate lab in Mie scattering](#)

[American Journal of Physics](#) **69**, 129 (2001); 10.1119/1.1311785

[Mie scattering](#)

[American Journal of Physics](#) **53**, 955 (1998); 10.1119/1.14011

[Verification of the Rayleigh scattering cross section](#)

[American Journal of Physics](#) **75**, 824 (2007); 10.1119/1.2752825

[Rayleigh scattering](#)

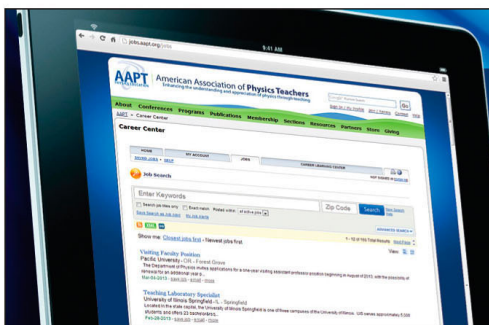
[Physics Today](#) **35**, 42 (2008); 10.1063/1.2890003

[Rayleigh, Mie, and Tyndall scatterings of polystyrene microspheres in water: Wavelength, size, and angle dependences](#)

[Journal of Applied Physics](#) **105**, 023110 (2009); 10.1063/1.3068473

[A simple demonstration of Mie scattering using an overhead projector](#)

[American Journal of Physics](#) **70**, 91 (2001); 10.1119/1.1412647



American Association of Physics Teachers

Explore the **AAPT Career Center** – access hundreds of physics education and other STEM teaching jobs at two-year and four-year colleges and universities.

<http://jobs.aapt.org>



An experiment to measure Mie and Rayleigh total scattering cross sections

A. J. Cox, Alan J. DeWeerd,^{a)} and Jennifer Linden
Department of Physics, University of Redlands, Redlands, California 92373

(Received 9 July 2001; accepted 7 February 2002)

We present an undergraduate-level experiment using a conventional absorption spectrophotometer to measure the wavelength dependence of light scattering from small dielectric spheres suspended in water. The experiment yielded total scattering cross-section values throughout the visible region that were in good agreement with theoretical values predicted by the Rayleigh and Mie theories.

© 2002 American Association of Physics Teachers.

[DOI: 10.1119/1.1466815]

I. INTRODUCTION

One of the most important examples of interaction at the microscopic scale is the phenomenon of scattering. For example, much of what has been learned about the structure of the nucleus, indeed even its discovery, was the result of scattering experiments. Similarly, the analysis of scattering has yielded most of our present knowledge of elementary particle physics. Compton scattering of x rays by electrons is often cited as experimental evidence for the particle nature of the photon. One of the earliest examples of scattering to be studied was that of light scattered by the atmosphere, which was studied by Tyndall, Rayleigh, and others at the end of the nineteenth century.¹ The wavelength dependence of scattering by the atmosphere is responsible for both the blue sky and red sunset.² Light scattering is of such great importance in optics that Mark P. Silverman wrote that, “virtually every aspect of physical optics is an example of light scattering.”³

Several light scattering experiments useful for teaching undergraduates have appeared in this journal. Ardgide, Pinnoch, and Collins measured the spectrum of light scattered by the atmosphere.⁴ Their measurements yielded the expected wavelength dependence of the spectrum of scattered light, but not absolute scattering cross sections. Experiments by Drake and Gordon⁵ and recent work by Weiner, Rust, and Donnelly,⁶ measured the angular distribution of light scattered from small particles at a single wavelength. They were able to fit their data to Mie theory calculations and accurately determine particle radii. Pastel *et al.*⁷ performed similar angular measurements with single liquid drops to determine their size.

This paper discusses an experiment that measures total light scattering cross sections for small particles throughout the visible spectrum using a conventional absorption spectrophotometer. Because this instrument is available in most chemistry departments, no special apparatus need be constructed. With this instrument absolute total cross sections can be easily obtained by undergraduate students in one laboratory period. The experimental cross sections agreed well with the exact Mie theory calculations, which were performed with an existing computer program. The smallest particles studied were sufficiently small so that their measured cross sections also agreed well with those calculated using the Rayleigh approximation. The concepts of scattering cross section and beam attenuation discussed in this paper may be extended to other types of scattering (for example, Compton and Rutherford scattering) prominent in the undergraduate curriculum.

II. THEORY

The Rayleigh cross section is valid for spherical particles that have radii small compared to the wavelength of the scattered light. Its derivation involves important concepts such as the definition of the scattering cross section, the polarization of a dielectric sphere, and radiation from a driven oscillating dipole. Because the derivation should be understood by students who perform this experiment, it is included as an appendix. For the Rayleigh approximation the cross section can be written as the analytic function,

$$\sigma_{\text{Ray}} = \frac{8\pi}{3} \left(\frac{2\pi n_{\text{med}}}{\lambda_0} \right)^4 a^6 \left(\frac{m^2 - 1}{m^2 + 2} \right)^2, \quad (1)$$

where λ_0 is the vacuum wavelength, a is the particle radius, and $m = n_{\text{sph}}/n_{\text{med}}$ is the ratio of the refractive index of the particle to that of the surrounding medium. The Rayleigh cross section is clearly proportional to λ_0^{-4} .

The Mie cross section, which is valid for spheres of any size, is obtained from a considerably more complicated calculation than the Rayleigh approximation. The details of its derivation are discussed in Refs. 8 and 9, and summaries of the calculation are in Refs. 6 and 10. The solution involves an incident plane wave and an outgoing spherical scattered wave. Because of the spherical symmetry of the system, the incident wave is expanded as an infinite series of vector spherical harmonics. The components of the total (incident plus scattered) electric and magnetic fields tangent to the surface of the sphere are required to be continuous across the boundary. After considerable mathematical manipulation, the scattered fields are determined and from these fields, the differential and total cross sections are found. The Mie total scattering cross section is expressed as the infinite series

$$\sigma_{\text{Mie}} = \left(\frac{2\pi}{k_{\text{med}}^2} \right) \sum_{n=1}^{\infty} (2n+1)(|a_n|^2 + |b_n|^2), \quad (2)$$

where $k_{\text{med}} = 2\pi n_{\text{med}}/\lambda_0$. The coefficients a_n and b_n are given by

$$a_n = \frac{\mu m^2 j_n(mx)[xj_n(x)]' - \mu_1 j_n(x)[mxj_n(mx)]'}{\mu m^2 j_n(mx)[xh_n^{(1)}(x)]' - \mu_1 h_n^{(1)}(x)[mxj_n(mx)]'},$$
$$b_n = \frac{\mu_1 j_n(mx)[xj_n(x)]' - \mu j_n(x)[mxj_n(mx)]'}{\mu_1 j_n(mx)[xh_n^{(1)}(x)]' - \mu h_n^{(1)}(x)[mxj_n(mx)]'},$$

where the j_n 's are spherical Bessel functions of the first kind, the h_n 's are spherical Hankel functions, and μ_1 and μ are the magnetic permeability of the sphere and surrounding me-

dium, respectively. For the present case $\mu_1 = \mu$, and hence they cancel. The quantity $x = (2\pi n_{\text{med}}a)/\lambda_0$ is called the size parameter and primes indicate derivatives with respect to x . Numerical values of σ_{Mie} were calculated using the subroutine BHME.¹¹ This computer code and similar ones are readily available online.¹² The series expression for σ_{Mie} converges after a number of terms slightly larger than the size parameter. For example, the largest particles studied, $a = 0.2615 \mu\text{m}$, required only five terms to converge to four significant figures for $x = 2.96$.

The commonly used criterion for the validity of the Rayleigh approximation is that $mx \ll 1$. To compare the behavior of σ_{Ray} and σ_{Mie} , calculations were performed over a range of values of mx . Figure 1 presents the results in terms of the respective scattering efficiencies, $Q = \sigma/\pi a^2$, versus mx . For the smallest particles, $a = 0.0285 \mu\text{m}$, with $mx = 0.57$ at 500 nm, the Rayleigh and Mie cross sections differ by only 5.4%. Thus even though the requirement of $mx \ll 1$ is not strictly satisfied for our smallest particles, the Rayleigh cross section is still a useful approximation for them. Figure 1 also demonstrates how drastically the predictions of the two theories differ for size parameters much larger than unity. For example, Mie theory predicts that the efficiency does not always rise as the size parameter increases, which means that for certain particle sizes the cross section will actually become larger with increasing wavelength.¹³ This behavior is in sharp contrast to the λ_0^{-4} wavelength dependence of the Rayleigh cross section.

For large x (that is, particle radius much larger than the wavelength), it might be expected from geometrical optics that the total cross section from the exact calculation (Mie theory) would be πa^2 , and thus Q would approach 1. However, Fig. 1 shows the interesting and somewhat puzzling trend that as x becomes large, the scattering efficiency approaches 2. This phenomenon is called the “extinction paradox” and is discussed in detail by van de Hulst¹⁴ and Bohren and Huffman.¹⁵ The result is apparent only for observations made far from an object, so that even light that is scattered at a small angle can be considered removed from the beam. The same paradox arises in quantum mechanical scattering in the limit $ka \gg 1$. The total cross section results from the geo-

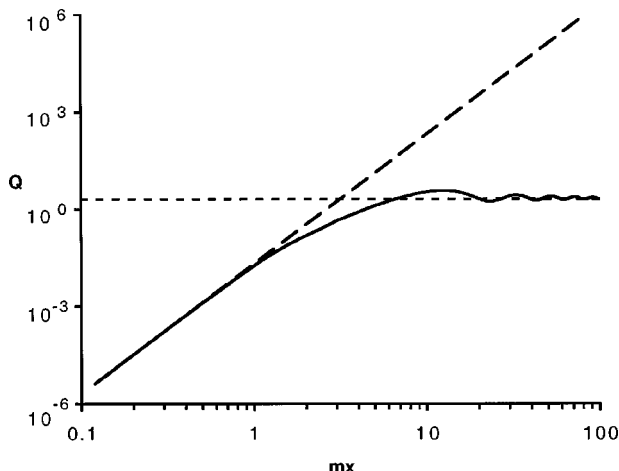


Fig. 1. Plot of scattering efficiencies, $Q = \sigma/\pi a^2$, for Rayleigh (dashed curve) and Mie (solid curve) scattering vs mx for $m=1.59/1.33$. The dotted line indicates the limiting value of $Q=2$.

metrical contribution (classical limit) of πa^2 and an equal contribution from the diffraction of the incident plane wave at the sharp edge of the sphere. The diffraction contribution is strongly peaked forward around a scattering angle of $\theta_{\text{max}} \approx 1/ka$. For nearby macroscopic objects this diffracted light is not distinguishable from unscattered light at $\theta=0$, and the paradox is not observed.¹⁶

III. EXPERIMENT

The experiment consists of measuring the attenuation of an unpolarized light beam as it passes through a sample of spherical particles suspended in water. The polystyrene spheres with refractive index $n_{\text{sph}} = 1.59$ were obtained from Duke Scientific Corporation.¹⁷ Particles with radii of $a = 0.0285, 0.0605$, and $0.2615 \mu\text{m}$ were studied. Samples of various number densities, ρ , were prepared based on the manufacturer’s specification that the purchased samples consisted of 10% particles by volume in water. As recommended by the manufacturer, the original sample container was placed in an ultrasonic bath for a few minutes to gently stir and distribute the particles evenly throughout the water. Then a measured amount of particles and water were added to distilled water to obtain suitable number densities.

The instrument used to measure the attenuation of light as a function of the wavelength was an absorption spectrophotometer.¹⁸ Before performing the experiment, students are asked to remove the outside cover of the instrument and compare the exposed optical components to the schematic diagram in Fig. 2. Light from a halogen lamp (L) is reflected and focused by a cylindrical mirror (M1) onto a slit (S1). After passing through the slit, the expanding beam is diffracted and refocused by a cylindrical grating (G) onto another slit (S2). The quasimonochromatic light from S2 with a spectral bandwidth of 2 nm is then collimated by a spherical mirror (M2) and divided into two beams by a beam splitter (BS). Mirrors (M3 and M4) direct the two beams through the sample cell (SC) and the reference cell (RC), which are identical 1-cm square quartz cells. The sample cell is filled with distilled water and suspended particles, and the reference cell contains only distilled water. After passing through the cells, the beams continue to matched silicon photodiode detectors (D1 and D2). The beam passing through the sample cell is attenuated due to scattering outside the approximately 3° cone angle subtended by the detector. The dual-beam instrument automatically subtracts out losses in

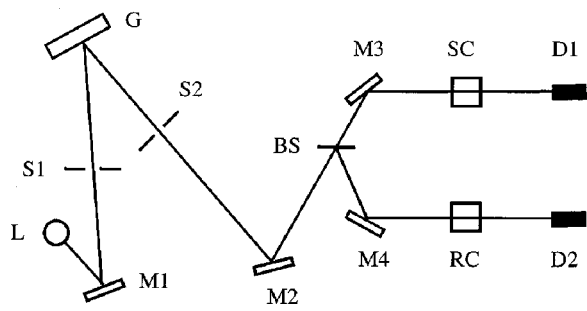


Fig. 2. A schematic diagram of the spectrophotometer. L is the light source, M1–M4 are mirrors, S1 and S2 are slits, G is the cylindrical grating, BS is the beam splitter, SC is the sample cell, RC is the reference cell, and D1 and D2 are detectors.

the reference cell due to reflection from the cell walls or absorption or scattering by the distilled water.

If the particle number density is sufficiently low, the light will most likely scatter only once in passing through the sample cell. Under these single scattering conditions, the reduced irradiance $I(L)$ after passing through a sample of length L is related to the initial beam irradiance I_0 by $I(L) = I_0 e^{-\rho\sigma L}$. The instrument actually records the optical density, D , of the sample. The optical density is a logarithmic measure of the beam attenuation defined by $D = \log(I_0/I(L))$, so the experimental cross section is given by

$$\sigma = (\ln 10)D/\rho L. \quad (3)$$

Absorption was negligible for the particles studied so σ is the scattering cross section.

It is necessary that the experiments be performed under conditions for which single scattering is the dominant attenuation process. Otherwise, some light scattered out of the original beam might be scattered again and reach the detector. This multiply scattered light would be incorrectly recorded as unscattered, and the final optical density and experimental cross section would be erroneously low. To study the effects of multiple scattering, measurements were made with decreasing number densities corresponding to optical densities from $D = 2.0$ to 0.1 at 500-nm wavelength. It was found that as D decreased, the experimental cross section rose to a constant maximum value for D below about 0.5. Therefore, it was assumed that for D below 0.5, multiple scattering could be ignored. The experimental cross sections reported in Sec. IV were obtained from samples with D between 0.1 and 0.5.

We consider the question of whether the present experiment could be performed using other suspensions, such as fat globules from milk. The spectrophotometer could measure the wavelength dependence of the attenuation due to the scattering and yield values of $\rho\sigma$ vs λ . These measurements would provide a quantitative complement to the common classroom demonstration that shows that blue light is scattered more than red by very small particles.¹⁹ However, the cross sections could not be determined because the number density, ρ , would be unknown. Similarly, the theoretical cross sections for these particles could not be calculated because the particle radii would also be unknown.

IV. RESULTS AND DISCUSSION

Experimental measurements were obtained for the three particle sizes mentioned previously. For each particle size, several experimental samples were prepared from the original sample supplied by the manufacturer. Repeated measurements on these samples produced run to run consistencies within about 2%. In the case of the smallest particle radius, a second sample obtained from the manufacturer also produced similar agreement with earlier experiments.

Figure 3 is a plot of experimental total cross sections compared with the Rayleigh cross section for a particle radius of $a = 0.0285 \mu\text{m}$. Even though this radius corresponds to $mx = 0.57$ at 500 nm, there was still good agreement between the Rayleigh theory and the experimental results. Figure 4 shows the experimental cross sections versus λ_0^{-4} ; the experimental results lie on a straight line with a slope of $(3.6 \pm 0.2) \times 10^{-43} \text{ m}^6$. This slope compares well with the Rayleigh theory prediction of $3.4 \times 10^{-43} \text{ m}^6$.

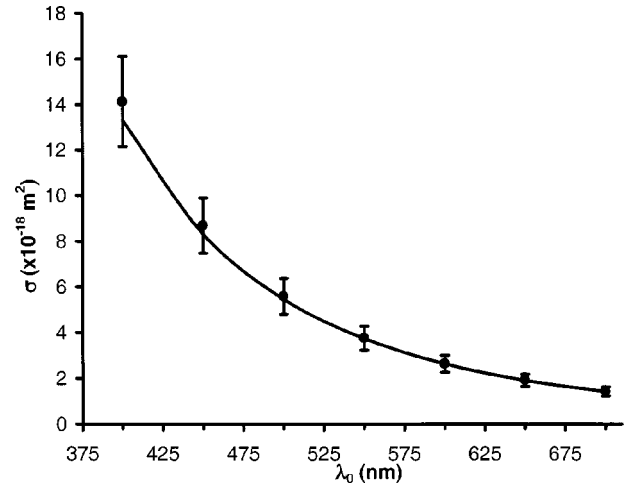


Fig. 3. Experimental cross sections (points) and Rayleigh cross section (solid line) vs the wavelength λ_0 for $a = 0.0285 \mu\text{m}$. The error bars represent the experimental uncertainties discussed in the text.

The particle radius of $a = 0.0605 \mu\text{m}$ corresponds to $mx = 1.21$ at 500 nm. For this mx value, Fig. 1 shows that Q_{Ray} exceeds Q_{Mie} by 28%. Figure 5 is a graph of experimental, Rayleigh, and Mie cross sections versus λ_0 . The experimental cross sections are in good agreement with the Mie theory, but not with the Rayleigh predictions, as expected. The experimental cross sections are plotted versus λ_0^{-4} for these particles in Fig. 6. The curve is seen to still be linear even though the particle radii are outside the range for the Rayleigh theory. However, the experimental slope of $(2.38 \pm 0.03) \times 10^{-41} \text{ m}^6$ does not agree with the value of $2.99 \times 10^{-41} \text{ m}^6$ predicted by the Rayleigh theory.

The largest particle radius, $a = 0.2615 \mu\text{m}$, with $mx = 4.7$ at 500 nm was well outside the range where the Rayleigh theory is valid and should only be compared to the Mie theory. Figure 7 shows good agreement between the wavelength dependence of the experimental and Mie theory cross sections. Figure 8 is a plot of the experimental cross section versus λ_0^{-4} , which is no longer linear. However, shorter

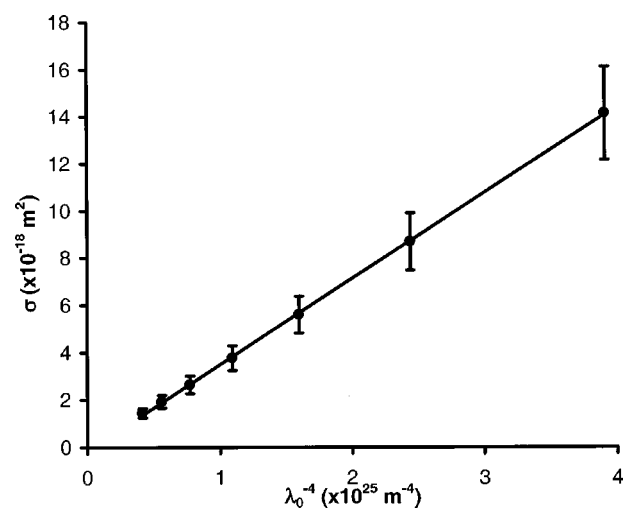


Fig. 4. Experimental cross sections vs λ_0^{-4} for particle radius $a = 0.0285 \mu\text{m}$ with a least-squares straight line fit.

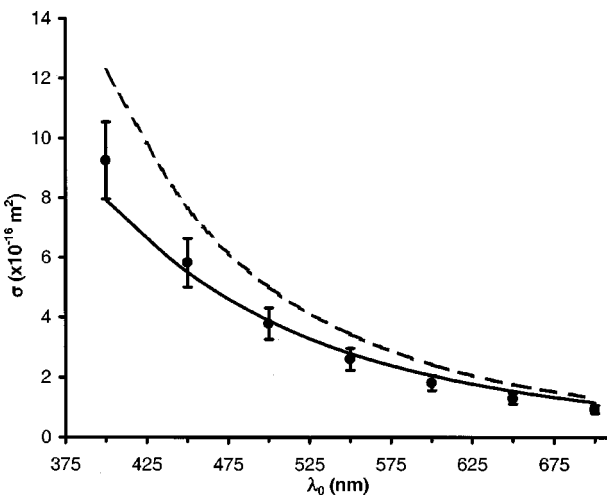


Fig. 5. Experimental (points), Rayleigh (dashed curve), and Mie (solid curve) cross sections vs λ_0 for $a=0.0605\text{ }\mu\text{m}$.

wavelengths are still scattered more than longer ones as expected for particles smaller than the wavelength.

There were several sources of uncertainty in both the experimental and the theoretical values displayed in the figures. The experimental cross sections were calculated from Eq. (3). The uncertainty in the number density, ρ , resulted from uncertainties in the average particle radius, $\langle a \rangle$, and in the fraction of particles by volume, f , in the original sample from the manufacturer. These values were specified by the manufacturer to be $\pm 4\%$ for $\langle a \rangle$ and $\pm 10\%$ for f . The measured optical density D had an estimated uncertainty of 2%, which resulted in an overall uncertainty value of $\pm 15.7\%$ in the experimental cross sections. This uncertainty is represented by the error bars in Figs. 3–8.

The theoretical Rayleigh cross section is proportional to a^6 , so an uncertainty of $\pm 4\%$ in $\langle a \rangle$ results in a 24% uncertainty in σ_{Ray} . Similar uncertainties are inherent in the cross sections calculated from the Mie theory. Table I shows experimental and appropriate theoretical cross sections together with the above uncertainties for the three-particle radii at

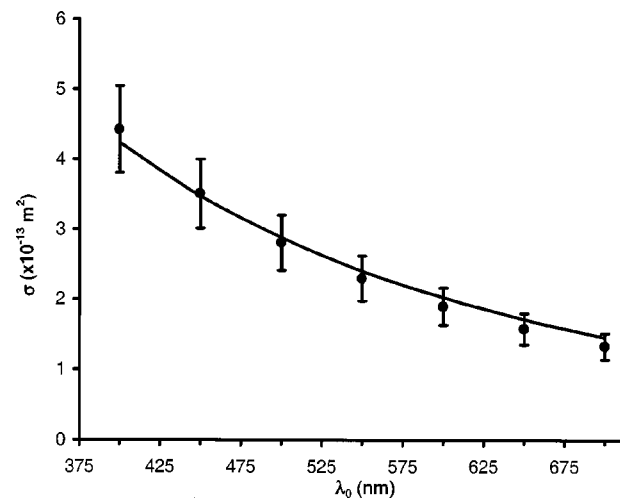


Fig. 7. Experimental cross sections (points) and Mie cross section (solid curve) vs λ_0 for $a=0.2615\text{ }\mu\text{m}$.

three wavelengths. For each particle size, the agreement between experiment and theory is within the uncertainty estimate.

There is another interesting consideration with regard to the particle radii used in these calculations. The manufacturer specified that a given sample was composed of particles of a certain mean radius, $\langle a \rangle$, with a standard deviation in size uniformity of σ_a . These σ_a values, expressed as a percent of $\langle a \rangle$, were 2.1%, 4.5%, and 15% for radii of 0.2615, 0.0605, and 0.0285 μm , respectively. Hence, the calculated cross sections should be calculated as an average over the appropriate size distribution function. The averaging was done analytically for the Rayleigh cross sections. Because σ_{Ray} is proportional to a^6 , the average effective cross section was found by replacing $\langle a \rangle^6$ by $\langle a^6 \rangle$, the average value of a^6 over the size distribution. If we assume that the distribution function is Gaussian, then $\langle a^6 \rangle$ is given by

$$\langle a^6 \rangle = \frac{1}{\sqrt{2\pi}\sigma_a} \int_{-\infty}^{+\infty} a^6 \exp[-(a - \langle a \rangle)^2 / 2\sigma_a^2] da. \quad (4)$$

Equation (4) yields

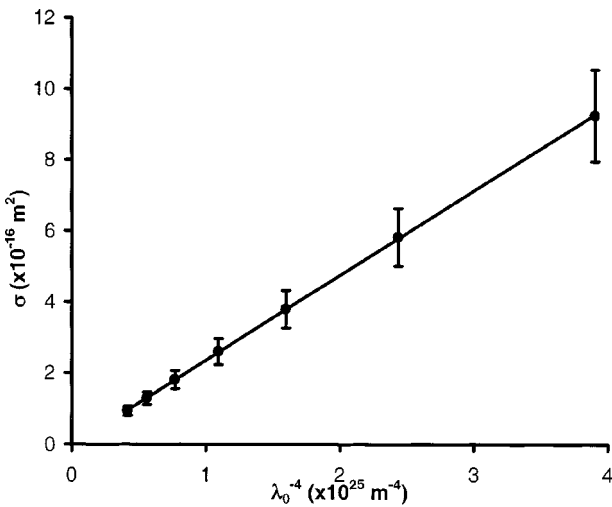


Fig. 6. Experimental cross sections vs λ_0^{-4} for $a=0.0605\text{ }\mu\text{m}$ with a least-squares straight line fit.

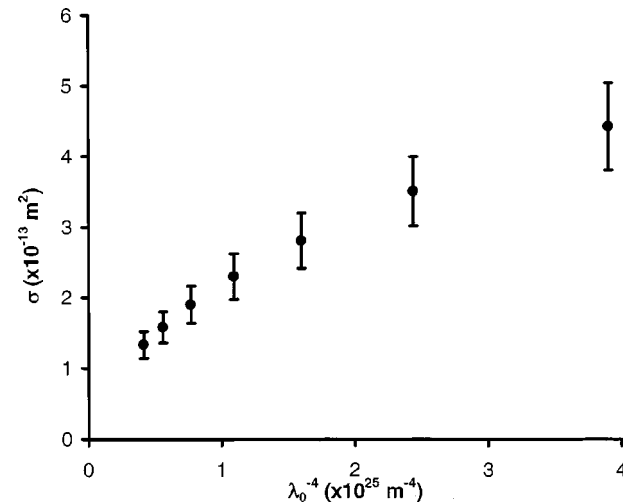


Fig. 8. Experimental cross sections vs λ_0^{-4} for $a=0.2615\text{ }\mu\text{m}$.

Table I. Experimental and Rayleigh or Mie cross sections with estimated uncertainties for three radii.

$a=0.0285 \mu\text{m}$		
λ_0 (nm)	$\sigma_{\text{exp}}(\text{m}^2)$	$\sigma_{\text{Rayleigh}}(\text{m}^2)$
450	$8.68 \pm 1.22 (\times 10^{-18})$	$8.32 \pm 2.00 (\times 10^{-18})$
550	$3.75 \pm 0.53 (\times 10^{-18})$	$3.73 \pm 0.90 (\times 10^{-18})$
650	$1.92 \pm 0.27 (\times 10^{-18})$	$1.91 \pm 0.46 (\times 10^{-18})$

$a=0.0605 \mu\text{m}$		
λ_0 (nm)	$\sigma_{\text{exp}}(\text{m}^2)$	$\sigma_{\text{Mie}}(\text{m}^2)$
450	$5.89 \pm 0.82 (\times 10^{-16})$	$5.50 \pm 1.32 (\times 10^{-16})$
550	$2.72 \pm 0.38 (\times 10^{-16})$	$2.79 \pm 0.67 (\times 10^{-16})$
650	$1.41 \pm 0.20 (\times 10^{-16})$	$1.53 \pm 0.37 (\times 10^{-16})$

$a=0.2615 \mu\text{m}$		
λ_0 (nm)	$\sigma_{\text{exp}}(\text{m}^2)$	$\sigma_{\text{Mie}}(\text{m}^2)$
450	$3.51 \pm 0.49 (\times 10^{-13})$	$3.47 \pm 0.83 (\times 10^{-13})$
550	$2.30 \pm 0.32 (\times 10^{-13})$	$2.40 \pm 0.58 (\times 10^{-13})$
650	$1.58 \pm 0.22 (\times 10^{-13})$	$1.71 \pm 0.41 (\times 10^{-13})$

$$\langle a^6 \rangle = \langle a \rangle^6 + 15\langle a \rangle^4 \sigma_a^2 + 45\langle a \rangle^2 \sigma_a^4 + 15\sigma_a^6. \quad (5)$$

Because $\sigma_a/\langle a \rangle$ is small, the fractional change in the Rayleigh cross section due to using $\langle a^6 \rangle$ rather than $\langle a \rangle^6$ is approximately $15(\sigma_a/\langle a \rangle)^2$. For $a=0.0285 \mu\text{m}$, the $\sigma_a/\langle a \rangle$ value of 15% should result in a 33% increase in the measured cross section. However, the experimental results for this particle size were in agreement to better than 5% with theoretical predictions based on the nominal values of $\langle a \rangle$, without making the above correction for this distribution. Our results were consistent with predictions based on a size distribution with $\sigma_a/\langle a \rangle$ of 5% or less. Therefore, we speculate that the width of the particle size distribution might have been smaller than 15%. Wang and Hallett have developed an inversion technique to extract particle size distributions from extinction spectra.²⁰ Although their methods are beyond the scope of the present study, they might be used to determine the size distribution for these particles.

The average of the Mie cross sections over the distribution of the particle radii cannot be calculated analytically. Therefore, the integral was found numerically using Gauss-Hermite quadrature.²¹ For a function weighted by a Gaussian, the integral may be approximated by

$$\int_{-\infty}^{+\infty} e^{-y^2} f(y) dy \approx \sum_n w_n f(y_n), \quad (6)$$

where y_n are the roots of the n th order Hermite polynomial and w_n are the associated weights.²² Six terms were sufficient to calculate the averaged cross sections to three significant figures. For $\lambda_0=500 \text{ nm}$, the $\sigma_a/\langle a \rangle$ percentages given above resulted in increases in the theoretical cross sections of only 2.3% and 0.2% for the radii of 0.2614 and $0.0605 \mu\text{m}$, respectively. These increases were insignificant compared to the other uncertainties in the theoretical values.

V. CONCLUSIONS

We have presented an experiment and analysis that could serve as a convenient introduction to light scattering from small, spherical particles in an undergraduate laboratory. If only the smallest particle size is studied, then the simple Rayleigh theory gives good agreement with experimental

measurements. These results yield clear confirmation that the cross section is proportional to λ_0^{-4} , as is often mentioned in introductory discussions of atmospheric light scattering. If studies are done with the larger particles, then the Mie theory is required. The Mie cross sections are easily calculated using existing programs, and there is good agreement between theory and experiment.

APPENDIX: DERIVATION OF THE RAYLEIGH CROSS SECTION

Figure 9 shows the electric field of a plane wave in vacuum traveling in the z direction, linearly polarized in the $x-z$ plane given by $\mathbf{E}(z,t)=\hat{x}E_0 \sin(k_0 z - \omega t)$, where $k_0 = 2\pi/\lambda_0$. The wave is incident on a dielectric sphere of radius a and real (nonabsorbing) refractive index n_{sph} . The probability that the sphere scatters radiation at angle θ is proportional to the differential scattering cross section, $d\sigma(\theta)/d\Omega$. Integrating $d\sigma(\theta)/d\Omega$ over all scattering angles yields the total scattering cross section, σ , which is proportional to the probability of scattering in any direction. The differential cross section is defined as the ratio of the power scattered into the solid angle, $d\Omega$, between θ and $\theta+d\theta$ to the incident power per unit area. The latter is the magnitude of the incident time averaged Poynting vector and is given by $|\langle \mathbf{S}_i \rangle| = E_0^2/2\mu_0 c$.

The scattered power results from the driven oscillating polarization of the dielectric sphere. The primary assumption involved in Rayleigh scattering is that the sphere diameter is considerably smaller than the wavelength inside the sphere so that the polarization, \mathbf{P} , can be approximated as uniform throughout the sphere. The usual criterion for this assumption to be satisfied is $n_{\text{sph}}k_0 a \ll 1$.²³ Under these conditions the entire sphere is considered to be an oscillating dipole of magnitude $\mathbf{P}_0 = \mathbf{P}(4\pi a^3/3)$. It is assumed that for visible light the frequency is low enough that resonance absorption in the ultraviolet can be neglected.

The polarization of the sphere is found by solving the classic problem of a dielectric sphere in a previously uniform field and is $\mathbf{P} = 3\epsilon_0 \mathbf{E}_0 (n_{\text{sph}}^2 - 1)/(n_{\text{sph}}^2 + 2)$.²⁴ The radiated (scattered) irradiance a distance r from the oscillating dipole at angle θ is $|\langle \mathbf{S}_s \rangle|_{\parallel} = (\mu_0 \omega^4 P_0^2) \cos^2 \theta / (32\pi^2 c r^2)$ for incident polarization parallel to the scattering plane (the $x-z$ plane), and $|\langle \mathbf{S}_s \rangle|_{\perp} = (\mu_0 \omega^4 P_0^2) / (32\pi^2 c r^2)$ for incident polarization perpendicular to the scattering plane.²⁵ For unpolarized incident light the total scattered irradiance is then the

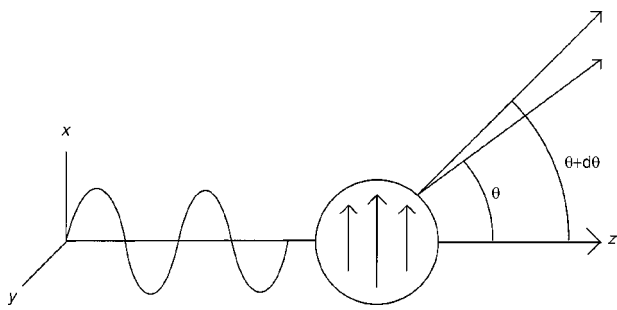


Fig. 9. A plane wave polarized in the $x-z$ plane is incident on the sphere from the left. Part of the scattered wave is scattered between θ and $\theta + d\theta$. The arrows on the sphere indicate the polarization, \mathbf{P} , of the dielectric material.

average over the two polarizations, $|\langle \mathbf{S}_s \rangle| = 1/2[|\langle \mathbf{S}_s \rangle|_{||} + |\langle \mathbf{S}_s \rangle|_{\perp}]$. Multiplying the irradiance by the area subtended by the solid angle $d\Omega$, $dA = r^2 d\Omega$, yields the total power scattered into the solid angle. Finally, by using the above definition of the differential cross section and substituting the total dipole moment of the sphere, we obtain

$$\frac{d\sigma(\theta)}{d\Omega} \Big|_{\text{Ray}} = \frac{1}{2} \left(\frac{n_{\text{sph}}^2 - 1}{n_{\text{sph}}^2 + 2} \right)^2 \left(\frac{2\pi}{\lambda_0} \right)^4 a^6 (1 + \cos^2 \theta).$$

For a sphere in a surrounding medium such as water with refractive index n_{med} , the index of the sphere is replaced by the relative index, $m = n_{\text{sph}}/n_{\text{med}}$, and the vacuum wavelength, λ_0 , is replaced by the wavelength in the medium, λ_0/n_{med} . The total scattering cross section is then obtained by integrating the above equation over the entire solid angle, which yields Eq. (1).

^aElectronic mail: Alan_DeWeerd@redlands.edu

¹Andrew T. Young, "Rayleigh scattering," *Phys. Today* **35** (1), 2–8 (1982).

²For a collection of research papers on light scattering by the atmosphere, see *Selected Papers on Scattering in the Atmosphere*, edited by Craig Bohren (SPIE Optical Engineering Press, Bellingham, WA, 1989).

³Mark P. Silverman, *Waves and Grains* (Princeton U.P., Princeton, NJ, 1998), pp. 288–290.

⁴Athanasis Aridgides, Ralph N. Pinnock, and Donald F. Collins, "Observation of Rayleigh scattering and airglow," *Am. J. Phys.* **44** (3), 244–247 (1976).

⁵R. M. Drake and J. E. Gordon, "Mie scattering," *Am. J. Phys.* **53** (10), 955–961 (1985).

⁶I. Weiner, M. Rust, and T. D. Donnelly, "Particle size determination: An undergraduate lab in Mie scattering," *Am. J. Phys.* **69** (2), 129–136 (2001).

⁷Robert Pastel, Akllan Struthers, Ryan Ringle, Jeremy Rogers, and Charles

Rohde, "Laser trapping of microscopic particles for undergraduate experiments," *Am. J. Phys.* **68** (11), 993–1001 (2000).

⁸H. C. van de Hulst, *Light Scattering by Small Particles* (Wiley, New York, 1957), p. 70.

⁹Craig F. Bohren and Donald R. Huffman, *Absorption and Scattering of Light by Small Particles* (Wiley, New York, 1983), pp. 82–129.

¹⁰Reference 3, pp. 288–290.

¹¹Reference 9, pp. 477–482.

¹²For example, <http://omlc.ogi.edu/software/mie/> has links to several sites, including the URL, http://omlc.ogi.edu/calc/mie_calc.html, where calculations can be done interactively online.

¹³Craig F. Bohren, *Clouds in a Glass of Beer: Simple Experiments in Atmospheric Physics* (Wiley, New York, 1987), pp. 91–97. This book contains an amusing anecdote about inadvertently demonstrating this behavior.

¹⁴Reference 8, pp. 107–108.

¹⁵Reference 9, pp. 107–111.

¹⁶Richard W. Robinett, *Quantum Mechanics: Classical Results, Modern Systems, and Visualized Examples* (Oxford U.P., New York, 1997), pp. 519–520.

¹⁷Duke Scientific Corporation, 2463 Faber Place, P.O. Box 50005, Palo Alto, CA 94303.

¹⁸Jasco Instruments, Model V530.

¹⁹Charles L. Adler and James A. Lock, "A simple demonstration of Mie scattering using an overhead projector," *Am. J. Phys.* **70** (1), 91–93 (2002).

²⁰Jianhong Wang and F. Ross Hallett, "Spherical particle size determination by analytical inversion of the UV-visible-NIR extinction spectrum," *Appl. Opt.* **35**, 193–197 (1996).

²¹S. E. Koonin, *Computational Physics* (Addison-Wesley, New York, 1986), pp. 83–87.

²²M. Abramowitz and I. A. Stegun, *Handbook of Mathematical Functions* (Dover, New York, 1965), p. 924.

²³Reference 9, pp. 132–134.

²⁴Roald K. Wangsness, *Electromagnetic Fields* (Wiley, New York, 1986), 2nd ed., p. 194.

²⁵J. D. Jackson, *Classical Electrodynamics* (Wiley, New York, 1975), 2nd ed., pp. 411–414.